Response of parametrically driven nonlinear coupled oscillators with application to micromechanical and nanomechanical resonator arrays

Ron Lifshitz
School of Physics and Astronomy, Raymond and Beverly Sackler Faculty of Exact Sciences, Tel Aviv University, Tel Aviv 69978, Israel

M. C. Cross
Condensed Matter Physics 114-36, California Institute of Technology, Pasadena, California 91125
(Received 21 August 2002; published 10 April 2003)

The response of a coupled array of nonlinear oscillators to parametric excitation is calculated in the weak nonlinear limit using secular perturbation theory. Exact results for small arrays of oscillators are used to guide the analysis of the numerical integration of the model equations of motion for large arrays. The results provide a qualitative explanation for a recent experiment [Buks and Roukes, J. Microelectromech. Syst. **11**, 802 (2002)] involving a parametrically excited micromechanical resonator array. Future experiments are suggested which could provide quantitative tests of the theoretical predictions.

DOI: 10.1103/PhysRevB.67.134302 PACS number(s): 85.85.+j, 05.45.−a, 05.45.Xt, 62.25.+g

I. MOTIVATION: NONLINEARITY OF MEMS AND NEMS RESONATORS

Recent technological advances have enabled the fabrication of mechanical resonators down to micrometer and even nanometer scales, with frequencies almost reaching the gigahertz range.[1,2] Even though the main thrust in this field of research comes from the need to produce smaller, lighter, faster, and more efficient electromechanical systems, there is new basic physics to be learned along the way.[3] One particularly interesting aspect of the physical behavior of microelectromechanical and nanoelectromechanical systems (MEMS and NEMS) is their nonlinear mechanical response at relatively small deviations from equilibrium. This nonlinear behavior has been observed experimentally,[2,4] and also exploited to achieve mechanical signal amplification and mechanical noise squeezing[5,7,6] in single resonators. In addition, MEMS and NEMS facilitates the fabrication of large arrays of resonators, for which the coherent response might be useful for signal enhancement and noise reduction. It is important to understand the nonlinear behavior of MEMS and NEMS resonators in order to improve their future designs. At the same time, one can take advantage of these systems for the experimental study of nonlinear dynamics.

This paper is motivated by a recent experiment by Buks and Roukes[8][henceforth BR] who fabricated an array of 67 fully suspended doubly clamped micromechanical resonating beams. Each beam was $270\times1\times0.25\mu$m in size, and the distance between neighboring beams was 4 μm. The substrate beneath the array was completely etched away, forming a suspended diffraction grating with optical access from both sides. All even-numbered beams were electrically connected to one electrode and all odd-numbered beams to a second electrode. This allowed the application of electrostatic forces to induce coupling between the beams. The system was driven parametrically by introducing an ac component to the potential difference between the even-numbered and odd-numbered beams. The collective response of the array, as a function of the driving frequency and the dc component of the potential difference, was measured using optical diffraction. The response that BR inferred from their measurement was surprising in that (i) instead of showing a band consisting of a sequence of resonance peaks at the 67 normal frequencies of the array, the typical response as the frequency was swept up showed a small number of wide peaks where the response gradually increased and very abruptly decreased; and (ii) the array responded at frequencies beyond the expected top edge of the band.

We show below that both these effects are a direct result of the fact that the restoring forces acting on the resonators as well as the damping that they undergo are both nonlinear. In Sec. II we describe the simplest equations of motion that are required to model the nonlinear resonator array. In Sec. III, we solve the response of a single nonlinear resonator to parametric excitation at twice its resonance frequency using secular perturbation theory (for comparison, we solve in Appendix A the response to parametric excitation at the resonance frequency). In Sec. IV we use the same method to calculate the response of the coupled resonator array and obtain exact results for a few (two or three) resonators. Understanding the analytical results of these two sections allows us to interpret the results of Sec. V, where we numerically integrate the equations of motion for an array of 67 resonators. Our results agree qualitatively with the observations of BR, explaining the two points mentioned above, but we suggest that further experiments be performed in order to test our theoretical calculations in a more quantitative manner.

II. EQUATIONS OF MOTION

We seek the simplest set of equations of motion (EOM) that capture the important physical aspects of the array of coupled micromechanical beams. We first note that the normal frequencies of an individual beam are sufficiently separated such that the frequency bands, formed by the coupling of the beams in the array, are well separated by gaps in which the system cannot respond. We therefore assume that we can treat the lowest band separately from all the others, so that each individual beam is oscillating strictly in its fun-

 ©2003 The American Physical Society

damental mode of vibration. Each beam can therefore be described by a single degree of freedom x_n, giving its displacement from equilibrium. We neglect any inhomogeneities in the fabrication of the beams and assume that all beams are identical. BR have actually examined each beam individually and report that their beams have a fairly uniform distribution of resonance frequencies, with an average of $\omega_B = 179.3$ kHz, and a standard deviation of 0.53 kHz. There is a much larger variation in the quality factors of the beams prior to the application of electrostatic interaction between them, but this variation disappears when a small potential difference is introduced between the beams.[9]

The coordinates x_n are all assumed to be small so that only terms to lowest order in x_n, necessary to capture the physical behavior of the system, will be kept in the EOM. Two types of forces act on the beams, namely, the elastic restoring force of each beam and the electrostatic forces between the beams. Experiments done by Buks and Roukes[4] on single beams of the type used in the array show that their response is similar to that of a Duffing oscillator—an oscillator whose restoring force contains a term proportional to the cube of the displacement and makes the oscillator stiffer than it would be within the harmonic approximation. Assuming a symmetric restoring force, and therefore no term proportional to an even power of x_n, and neglecting higher than cubic-order nonlinear corrections, the elastic force acting on the nth individual beam is

$$F^{(n)}_{elastic} = -m\omega_B^2 x_n - m\alpha x_n^3, \tag{1}$$

where m is the effective mass of a beam oscillating in its fundamental mode, whose frequency is ω_B.

Even though the electrostatic force between two parallel charged wires decays only as $1/r$, for simplicity we consider only the attractive interactions between nearest-neighbor beams. Within this approximation, each term in the EOM depends either on the variables x_n, describing the displacement of an individual beam from its equilibrium position, or on the difference variables $x_{n+1} - x_n$, describing the relative displacements of a pair of neighboring beams. To keep the equations as simple as possible, we restrict each type of nonlinear term in the EOM to depend either on x_n or on $x_{n+1} - x_n$, depending on whether it is mostly influenced by the elastic forces of the beams or the electrostatic interaction between them, respectively.

The cubic term in the expansion of the nearest-neighbor electrostatic interaction tends to pull the beams away from equilibrium, acting against the cubic term in the expansion of the elastic force in Eq. (1). Since, as we shall confirm later, the response of the array is consistent with having a cubic term that stiffens the beams, the elastic contribution to the cubic term is stronger than the electrostatic one. We therefore ignore the cubic as well as all higher terms in the electrostatic interaction, which we write as

$$F^{(n)}_{electric} = -\frac{1}{2} m\Delta^2 [1 + H\cos\omega_p t](x_{n+1} - 2x_n + x_{n-1}). \tag{2}$$

Note that the linear electrostatic force constant $\frac{1}{2}m\Delta^2$, which is modulated with a relative amplitude $H \ll 1$, representing the dc and the ac components of the applied voltage, is positive, acting to soften the elastic restoring force. The factor of 1/2 is used with the difference variable for convenience.

Parametric excitation, as it appears in the bare Mathieu equation for a single oscillator of frequency ω_0 without all the additional terms that we have here, is an instability of the system that occurs whenever the drive frequency is around one of the special values $\omega_p = 2\omega_0/n$, where n is an integer that labels the so-called instability tongues of the system (named after the tongue-shaped instability curves in the frequency-amplitude plane).[10] We choose the parametric driving frequency ω_p to be around twice some value ω_0 within the array's band of normal frequencies. We are therefore exciting the system in its first $(n=1)$ instability tongue. Thus,

$$\omega_p = 2\omega_0 + \epsilon\Omega, \tag{3}$$

where ϵ is a small parameter. In the BR experiment, the system was actually excited in its second instability tongue, i.e., ω_p was chosen around some frequency in the band. It turns out that the response at the second tongue, apart from a few differences, is quite similar to that of the first tongue. We therefore prefer to carry out full calculations only for the first tongue that is somewhat easier to handle, and just for comparison, we calculate in Appendix A the response of a single nonlinear oscillator, excited at its second tongue.

There is good reason to believe that most of the dissipation in the coupled system is a result of the electrostatic interaction that causes currents to flow through the beams. This assumption is based on the observation of Buks and Roukes[9] that the quality factors greatly diminish as the dc component of the electrostatic potential is increased. We therefore make the simplifying approximation that dissipation occurs predominantly as a result of currents, all other dissipation mechanisms being relatively negligible. This approximation avoids the problem of the variation in the quality factors of the individual beams before application of the electrostatic potential. The dissipative forces in the EOM are therefore written with respect to the difference variable,

$$\begin{aligned} F^{(n)}_{diss} = {} & \frac{1}{2} m\omega_B \Gamma(\dot{x}_{n+1} - 2\dot{x}_n + \dot{x}_{n-1}) \\ & + \frac{1}{2} m\omega_B \alpha\eta[(x_{n+1} - x_n)^2(\dot{x}_{n+1} - \dot{x}_n) \\ & - (x_n - x_{n-1})^2(\dot{x}_n - \dot{x}_{n-1})], \end{aligned} \tag{4}$$

where we have included a nonlinear contribution to the dissipation, of the same order as the nonlinear elastic force (1). When putting all the pieces together, we (a) divide out the effective mass m of a beam; (b) scale time $t \to t/\omega_B$ so that all frequencies (including Δ) are measured in units of ω_B; and (c) scale length $x \to x/\sqrt{\alpha}$ to get rid of the dependence on α. The equation of motion for the nth beam becomes

$$\ddot{x}_n + x_n + x_n^3 + \frac{1}{2}\Delta^2[1 + H\cos(2\omega_0 + \epsilon\Omega)t] \times (x_{n+1} - 2x_n + x_{n-1}) - \frac{1}{2}\Gamma(\dot{x}_{n+1} - 2\dot{x}_n + \dot{x}_{n-1}) - \frac{1}{2}\eta[(x_{n+1} - x_n)^2(\dot{x}_{n+1} - \dot{x}_n) - (x_n - x_{n-1})^2(\dot{x}_n - \dot{x}_{n-1})] = 0. \quad (5)$$

In the following sections, we shall solve these equations using secular perturbation theory. The physical parameter that allows us to use this approach is the linear damping coefficient which is assumed to be small. We therefore express it as $\Gamma = \epsilon\gamma$, taking ϵ to be our small expansion parameter. The parametric instability of the system then occurs for small driving amplitude near resonance, and if, in addition, we consider the system near the onset of the instability, we can assume that the effects of nonlinearity are small as well. Thus, for small displacements x_n, all the nontrivial physical effects, namely, the parametric excitation, the cubic elastic restoring force, and both the linear and the amplitude-dependent dissipation, all enter the EOM as perturbative corrections to the simple linear equations. All these perturbative terms can be chosen to enter the EOM in the same order of the small parameter ϵ by taking the leading order in x_n to be of the order of $\epsilon^{1/2}$, and expressing $\Delta^2 H = \epsilon h$. This ensures, as we shall confirm later on, that all the terms will contribute to the lowest-order solution we are seeking. The final form of the EOM is therefore

$$\ddot{x}_n + x_n + x_n^3 + \frac{1}{2}[\Delta^2 + \epsilon h\cos(2\omega_0 + \epsilon\Omega)t] \times (x_{n+1} - 2x_n + x_{n-1}) - \frac{1}{2}\epsilon\gamma(\dot{x}_{n+1} - 2\dot{x}_n + \dot{x}_{n-1}) - \frac{1}{2}\eta[(x_{n+1} - x_n)^2(\dot{x}_{n+1} - \dot{x}_n) - (x_n - x_{n-1})^2(\dot{x}_n - \dot{x}_{n-1})] = 0. \quad (6)$$

As for boundary conditions, we follow the experiment of BR who had two additional fixed beams, identical to all the rest, at both ends of the array. This means that we define two extra variables and set them to zero, $x_0 = x_{N+1} = 0$.

III. RESPONSE OF A SINGLE PARAMETRICALLY DRIVEN NONLINEAR OSCILLATOR

We begin by calculating the response of a single nonlinear oscillator to parametric excitation. Previous calculations of this problem exist in the literature[11] (and references therein), nevertheless, we solve it here as a precursor to the many-oscillator case, treated in the following section. The equation of motion (6) for the single-oscillator case becomes

$$\ddot{x} + [\omega^2 - \epsilon h\cos(2\omega + \epsilon\Omega)t]x + \epsilon\gamma\dot{x} + x^3 + \eta x^2\dot{x} = 0, \quad (7)$$

where we choose ω_0 to be $\omega = \sqrt{1 - \Delta^2}$, the resonance frequency of the beam in the harmonic approximation. The parametric excitation is performed around twice the actual resonance frequency of the oscillator. (In Appendix A, we treat the case where the excitation is performed around the resonance frequency of the resonator.)

We calculate the correction to linear response by using secular perturbation theory.[12,13] Recalling that the motion of the oscillator away from equilibrium is of the order of $\epsilon^{1/2}$, we try a solution of the form

$$x(t) = \epsilon^{1/2}(A(T)e^{i\omega t} + \text{c.c.}) + \epsilon^{3/2}x_1(t) + \cdots, \quad (8)$$

where $T = \epsilon t$ is a slow time variable, allowing the complex amplitude $A(T)$ to vary slowly in time. The variation of $A(T)$ gives us the extra freedom to eliminate secular terms and ensure that the perturbative correction $x_1(t)$, as well as all higher-order corrections to the linear response, do not diverge (as they do if one uses naive perturbation theory). Using the relation

$$\dot{A} = \frac{dA}{dt} = \epsilon\frac{dA}{dT} \equiv \epsilon A', \quad (9)$$

we calculate the time derivatives of the trial solution (8),

$$\dot{x} = \epsilon^{1/2}([i\omega A + \epsilon A']e^{i\omega t} + \text{c.c.}) + \epsilon^{3/2}\dot{x}_1(t) + \cdots, \quad (10a)$$

$$\ddot{x} = \epsilon^{1/2}([-\omega^2 A + 2i\omega\epsilon A' + \epsilon^2 A'']e^{i\omega t} + \text{c.c.}) + \epsilon^{3/2}\ddot{x}_1(t) + \cdots. \quad (10b)$$

Substituting these expressions back into the equation of motion (7), and picking out all terms of the order of $\epsilon^{3/2}$, we get the following equation for the first perturbative correction

$$\ddot{x}_1 + \omega^2 x_1 = -(2i\omega A' e^{i\omega t} + \text{c.c.}) + h\cos[(2\omega + \epsilon\Omega)t](Ae^{i\omega t} + \text{c.c.}) - \gamma(i\omega Ae^{i\omega t} + \text{c.c.}) - (Ae^{i\omega t} + \text{c.c.})^3 - \eta(Ae^{i\omega t} + \text{c.c.})^2(i\omega Ae^{i\omega t} + \text{c.c.}). \quad (11)$$

The collection of terms proportional to $e^{i\omega t}$ on the right-hand side of Eq. (11), called the secular terms, act like a force, driving the simple harmonic oscillator on the left-hand side at its resonance frequency. The sum of all the secular terms must vanish so that the perturbative correction $x_1(t)$ will not diverge. This gives us an equation for determining the slowly varying amplitude $A(T)$. After expressing the cosine as a sum of exponentials, we get

$$2i\omega\frac{dA}{dT} - \frac{h}{2}A^* e^{i\Omega T} + i\omega\gamma A + 3|A|^2 A + i\omega\eta|A|^2 A = 0. \quad (12)$$

Ignoring initial transients, and assuming that the nonlinear terms in the equation are sufficient to saturate the growth of the instability, we try a steady-state solution of the form

$$A(T) = ae^{i(\Omega/2)T}. \quad (13)$$

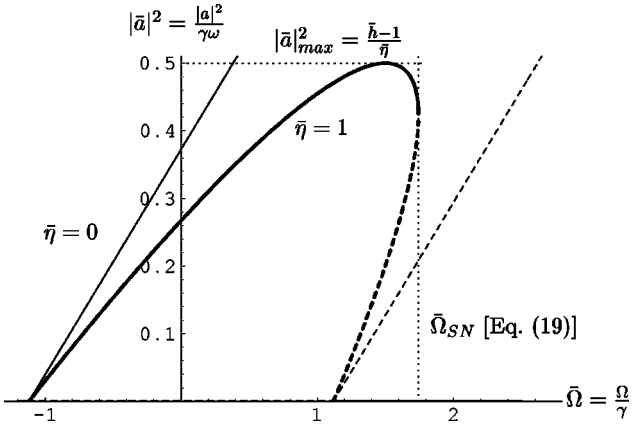

FIG. 1. Response intensity $|\bar{a}|^2$ as a function of the frequency $\bar{\Omega}$ for fixed amplitude $\bar{h}=1.5$. Solid curves are stable solutions and dashed curves are unstable solutions. Thin curves show the response without nonlinear damping ($\bar{\eta}=0$). Thick curves show the response for finite nonlinear damping ($\bar{\eta}=1$). Dotted lines indicate the maximal response intensity $|\bar{a}|^2_{max}$ and the saddle-node frequency $\bar{\Omega}_{SN}$.

The solution to the equation of motion (7) is therefore

$$x(t)=\epsilon^{1/2}(ae^{i(\omega+\epsilon\Omega/2)t}+\text{c.c.})+O(\epsilon^{3/2}), \tag{14}$$

where we are not interested in the correction $x_1(t)$ of the order of $\epsilon^{3/2}$, but rather in the fixed amplitude a of the lowest-order term. This amplitude a can be any solution of the equation

$$[(3|a|^2-\omega\Omega)+i\omega(\gamma+\eta|a|^2)]a=\frac{h}{2}a^*, \tag{15}$$

obtained by substituting the steady-state solution (13) into Eq. (12) of the secular terms. We immediately see that having no response ($a=0$) is always a possible solution regardless of the excitation frequency Ω. We divide both sides of Eq. (15) by $\gamma\omega$ and define the rescaled variables $\bar{a}=a/\sqrt{\gamma\omega}$, $\bar{\Omega}=\Omega/\gamma$, $\bar{\eta}=\omega\eta$, and $\bar{h}=h/2\gamma\omega$, in terms of which the equation for the fixed complex amplitude a becomes

$$[(3|\bar{a}|^2-\bar{\Omega})+i(1+\bar{\eta}|\bar{a}|^2)]\bar{a}=\bar{h}\bar{a}^*. \tag{16}$$

Expressing $\bar{a}=|\bar{a}|e^{i\phi}$ we obtain, after taking the magnitude squared of both sides, the intensity $|\bar{a}|^2$ of the nontrivial response as all positive roots of the equation

$$(3|\bar{a}|^2-\bar{\Omega})^2+(1+\bar{\eta}|\bar{a}|^2)^2=\bar{h}^2. \tag{17}$$

This has the form of a distorted ellipse in the $(\bar{\Omega},|\bar{a}|^2)$ plane, and a parabola in the $(|\bar{a}|^2,\bar{h})$ plane. In addition, we obtain for the relative phase of the response

$$\phi=\frac{i}{2}\ln\frac{\bar{a}^*}{\bar{a}}=-\frac{1}{2}\arctan\frac{1+\bar{\eta}|\bar{a}|^2}{3|\bar{a}|^2-\bar{\Omega}}. \tag{18}$$

In Fig. 1, we plot the response intensity $|\bar{a}|^2$ of a single oscillator to parametric excitation as a function of frequency $\bar{\Omega}$, for fixed amplitude $\bar{h}=1.5$, in terms of the rescaled variables. Solid curves indicate stable solutions and dashed curves are solutions that are unstable to small perturbations. Thin curves show the response without nonlinear damping ($\bar{\eta}=0$) which grows indefinitely with frequency $\bar{\Omega}$ and is therefore incompatible with the experimental observations of BR and the assumptions of our calculation. Thick curves show the response with finite nonlinear damping ($\bar{\eta}=1$). With finite $\bar{\eta}$, there is a maximum value for the response $|\bar{a}|^2_{max}=(\bar{h}-1)/\bar{\eta}$ and a maximum frequency

$$\bar{\Omega}_{SN}=\bar{h}\sqrt{1+\left(\frac{3}{\bar{\eta}}\right)^2}-\frac{3}{\bar{\eta}}, \tag{19}$$

at which the stability of the solution changes (known as a saddle-node bifurcation). For frequencies above $\bar{\Omega}_{SN}$ the only solution is the trivial one $\bar{a}=0$. These values are indicated by horizontal and vertical dotted lines in Fig. 1.

The threshold for the instability of the trivial solution is easily calculated by setting $\bar{a}=0$ in the expression (17) for the nontrivial solution. As seen in Fig. 1, for a given $\bar{h}$, the threshold is situated at $\bar{\Omega}=\pm\sqrt{\bar{h}^2-1}$. The threshold is plotted in Fig. 2 in the (Ω,h) plane. Note that the minimal amplitude needed for instability is obtained on resonance ($\bar{\Omega}=0$) and its value is $\bar{h}=1$, or $h=2\gamma\omega$, so that it scales as the linear damping coefficient γ.

Finally, in Fig. 3, we plot the response intensity $|\bar{a}|^2$ of the oscillator as a function of amplitude $\bar{h}$ for fixed frequency $\bar{\Omega}$ and finite nonlinear damping $\bar{\eta}=1$. Again, solid curves indicate stable solutions and dashed curves unstable solutions. Thick curves show the response for $\bar{\Omega}=1$ and thin curves show the response for $\bar{\Omega}=\bar{\eta}/3$ and $\bar{\Omega}=-1$. The intersection of the trivial and the nontrivial solutions, which corresponds to the instability threshold occurs at $\bar{h}=\sqrt{\bar{\Omega}^2+1}$. For $\bar{\Omega}<\bar{\eta}/3$ the nontrivial solution for $|\bar{a}|^2$ grows continuously for $\bar{h}$ above threshold and is stable. This is a supercritical bifurcation. On the other hand, for $\bar{\Omega}>\bar{\eta}/3$, the bifurcation is subcritical—the nontrivial solution grows for $\bar{h}$ *below* threshold. This solution is unstable until the curve of $|\bar{a}|^2$ as a function of $\bar{h}$ bends around at a saddle-node bifurcation at

$$\bar{h}_{SN}=\frac{1+\frac{\bar{\eta}}{3}\bar{\Omega}}{\sqrt{1+\left(\frac{\bar{\eta}}{3}\right)^2}}, \tag{20}$$

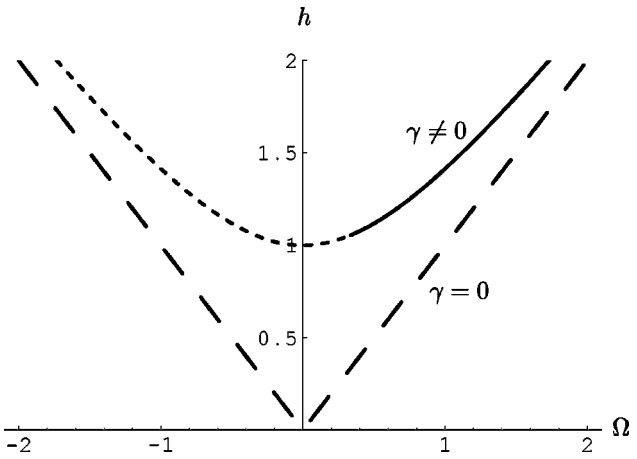

FIG. 2. Threshold for instability plotted in the (Ω,h) plane. The lower, long-dashed curve shows the threshold without any linear damping ($\gamma=0$), which is zero on resonance. The upper curve shows the threshold with linear damping ($\gamma\neq 0$). The parameters for the upper curve are $\omega=1/2$ and $\gamma=1$ so that $\bar{h}=h$. The threshold on resonance ($\bar{\Omega}=\Omega=0$) is therefore $\bar{h}=h=1$. The solid and short-dashed regions of the upper curve indicate the so-called subcritical and supercritical branches of the instability, respectively. On the subcritical branch ($\bar{\Omega}>\bar{\eta}/3$), there will be hysteresis as h is varied and on the supercritical branch ($\bar{\Omega}<\bar{\eta}/3$), there will not be any hysteresis.

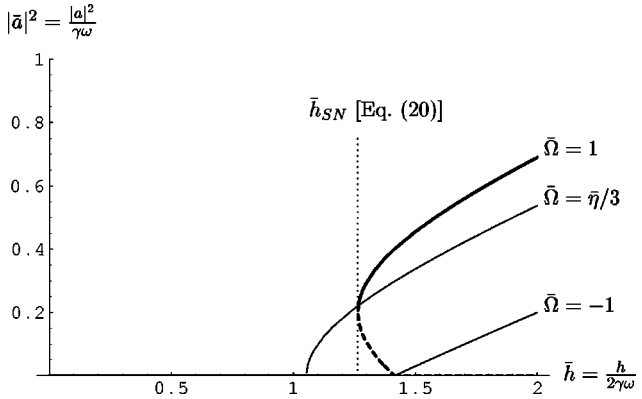

FIG. 3. Response intensity $|\bar{a}|^2$ as a function of the parametric modulation amplitude $\bar{h}$ for fixed frequency $\bar{\Omega}$ and finite nonlinear damping ($\bar{\eta}=1$). Thick curves show the stable (solid curves) and unstable (dashed curves) response for $\bar{\Omega}=1$. Thin curves show the stable solutions for $\bar{\Omega}=\bar{\eta}/3$ and $\bar{\Omega}=-1$, and demonstrate that hysteresis as $\bar{h}$ is varied is expected only for $\bar{\Omega}>\bar{\eta}/3$.

where the solution becomes stable and $|\bar{a}|^2$ is once more an increasing function of $\bar{h}$. For amplitudes $\bar{h}<\bar{h}_{SN}$, the only solution is the trivial one $\bar{a}=0$.

Like the response of a forced Duffing oscillator, the response of a parametrically excited Duffing oscillator also exhibits hysteresis in a frequency scan. If the frequency $\bar{\Omega}$ starts out at negative values and is increased gradually with a fixed amplitude $\bar{h}$, the response will gradually increase along the thick solid curve in Fig. 1, until $\bar{\Omega}$ reaches $\bar{\Omega}_{SN}$ and the response drops abruptly to zero. If the frequency is then decreased gradually, the response will remain zero until $\bar{\Omega}$ reaches the upper instability threshold $\sqrt{\bar{h}^2-1}$, and the response will jump abruptly to the thick solid curve above, and then gradually decrease to zero along this curve. A similar hysteretic behavior will be observed if the amplitude $\bar{h}$ is varied with a fixed frequency $\bar{\Omega}>\bar{\eta}/3$, as can be inferred from Fig. 3.

IV. RESPONSE OF A PARAMETRICALLY DRIVEN ARRAY OF NONLINEAR COUPLED OSCILLATORS—SECULAR PERTURBATION THEORY

Consider now the coupled array of nonlinear oscillators as described by the general EOM (6). We calculate its response to parametric excitation, again using secular perturbation theory. We expand $x_n(t)$ as a sum of standing-wave modes with slowly varying amplitudes

$$x_n(t)=\epsilon^{1/2}\sum_{m=1}^{N}(A_m(T)\sin(nq_m)e^{i\omega_m t}+\text{c.c.}) + \epsilon^{3/2}x_n^{(1)}(t)+\cdots, \quad n=1,\ldots,N. \tag{21}$$

Recall that the boundary conditions are such that there are two additional fixed beams, labeled 0 and $N+1$, exerting electrostatic forces on the first and the last beams of the array. With these boundary conditions ($x_0=x_{N+1}=0$), the possible wave vectors q_m are given by

$$q_m=\frac{m\pi}{N+1}, \quad m=1,\ldots,N. \tag{22}$$

We substitute the trial solution (21) into the EOM term by term. Up to order $\epsilon^{3/2}$, we have

$$\ddot{x}_n=\epsilon^{1/2}\sum_m \sin(nq_m)([-\omega^2A_m+2i\omega\epsilon A_m']e^{i\omega_m t}+\text{c.c.})+\epsilon^{3/2}\ddot{x}_n^{(1)}(t), \tag{23a}$$

$$x_{n+1}-2x_n+x_{n-1}=-4\epsilon^{1/2}\sum_m \sin^2\left(\frac{q_m}{2}\right)\sin(nq_m)(A_m e^{i\omega_m t}+\text{c.c.})+\epsilon^{3/2}(x_{n+1}^{(1)}-2x_n^{(1)}+x_{n-1}^{(1)}), \tag{23b}$$

$$\frac{1}{2}\epsilon\gamma(\dot{x}_{n+1}-2\dot{x}_n+\dot{x}_{n-1})=-2\epsilon^{3/2}\gamma\sum_m \omega_m\sin^2\left(\frac{q_m}{2}\right)\sin(nq_m)(iA_m e^{i\omega_m t}+\text{c.c.}), \tag{23c}$$

$$x_n^3=\epsilon^{3/2}\sum_{j,k,l}\sin(nq_j)\sin(nq_k)\sin(nq_l)(A_je^{i\omega_j t}+\text{c.c.})(A_ke^{i\omega_k t}+\text{c.c.})(A_le^{i\omega_l t}+\text{c.c.})$$

$$=\frac{\epsilon^{3/2}}{4}\sum_{j,k,l}\{\sin[n(-q_j+q_k+q_l)]+\sin[n(q_j-q_k+q_l)]+\sin[n(q_j+q_k-q_l)]-\sin[n(q_j+q_k+q_l)]\}$$

$$\times\{A_jA_kA_le^{i(\omega_j+\omega_k+\omega_l)t}+3A_jA_kA_l^*e^{i(\omega_j+\omega_k-\omega_l)t}+\text{c.c.}\},\tag{23d}$$

and

$$\frac{1}{2}\eta[(x_{n+1}-x_n)^2(\dot{x}_{n+1}-\dot{x}_n)-(x_n-x_{n-1})^2(\dot{x}_n-\dot{x}_{n-1})]$$

$$=-2\eta\epsilon^{3/2}\sum_{j,k,l}\sin\frac{q_j}{2}\sin\frac{q_k}{2}\sin\frac{q_l}{2}\left\{\sin\left[\frac{-q_j+q_k+q_l}{2}\right]\sin[n(-q_j+q_k+q_l)]+\sin\left[\frac{q_j-q_k+q_l}{2}\right]\sin[n(q_j-q_k+q_l)]\right.$$

$$\left.+\sin\left[\frac{q_j+q_k-q_l}{2}\right]\sin[n(q_j+q_k-q_l)]+\sin\left[\frac{q_j+q_k+q_l}{2}\right]\sin[n(q_j+q_k+q_l)]\right\}$$

$$\times(A_je^{i\omega_j t}+\text{c.c.})(A_ke^{i\omega_k t}+\text{c.c.})(i\omega_lA_le^{i\omega_l t}+\text{c.c.}).\tag{23e}$$

At the order of $\epsilon^{1/2}$, we simply get the linear dispersion relation, given by

$$\omega_m^2=1-2\Delta^2\sin^2\left(\frac{q_m}{2}\right),\quad m=1,\ldots,N.\tag{24}$$

At the order of $\epsilon^{3/2}$, we get N equations of the form

$$\ddot{x}_n^{(1)}+x_n^{(1)}+\frac{1}{2}\Delta^2(x_{n+1}^{(1)}-2x_n^{(1)}+x_{n-1}^{(1)})$$

$$=\sum_m\ (m\text{th secular term})e^{i\omega_m t}+\text{other terms},\tag{25}$$

where the left-hand sides are, again, coupled linear harmonic oscillators, with a dispersion relation given by Eq. (24). On the right-hand sides, we have N secular terms that act to drive the coupled oscillators $x_n^{(1)}$ at their resonance frequencies. As we did for a single oscillator in Sec. III, here too we require that all the secular terms vanish so that the $x_n^{(1)}$ remain finite, and thus obtain equations for the slowly varying amplitudes $A_m(T)$. To extract the equation for the mth amplitude $A_m(T)$, we make use of the orthogonality of the modes, multiplying all the terms by $\sin(nq_m)$ and summing over n. We also express all normal frequencies relative to the same reference frequency ω_0, used to define the excitation frequency ω_p in Eq. (3), so that

$$\omega_m=\omega_0+\epsilon\Omega_m.\tag{26}$$

We find that the coefficient of the mth secular term, which is required to vanish, is given by

$$-2i\omega_m\frac{dA_m}{dT}-2i\gamma\omega_m\sin^2\left(\frac{q_m}{2}\right)+hA_m^*\sin^2\left(\frac{q_m}{2}\right)e^{i(\Omega-2\Omega_m)T}$$

$$-\frac{3}{4}\sum_{j,k,l}A_jA_kA_l^*e^{i(\Omega_j+\Omega_k-\Omega_l-\Omega_m)T}\Delta_{jkl;m}^{(1)}$$

$$-2\eta\sum_{j,k,l}\left\{[2i\omega_lA_j^*A_kA_le^{i(-\Omega_j+\Omega_k+\Omega_l-\Omega_m)T}\right.$$

$$-i\omega_lA_jA_kA_l^*e^{i(\Omega_j+\Omega_k-\Omega_l-\Omega_m)T}]$$

$$\left.\times\Delta_{jkl;m}^{(2)}\sin\frac{q_j}{2}\sin\frac{q_k}{2}\sin\frac{q_l}{2}\sin\frac{q_m}{2}\right\}=0,\tag{27}$$

where we have introduced two Δ functions, defined in terms of Kronecker deltas as

$$\Delta_{jkl;m}^{(1)}=\delta_{-j+k+l,m}-\delta_{-j+k+l,-m}-\delta_{-j+k+l,2(N+1)-m}$$
$$+\delta_{j-k+l,m}-\delta_{j-k+l,-m}-\delta_{j-k+l,2(N+1)-m}$$
$$+\delta_{j+k-l,m}-\delta_{j+k-l,-m}-\delta_{j+k-l,2(N+1)-m}$$
$$-\delta_{j+k+l,m}+\delta_{j+k+l,2(N+1)-m}-\delta_{j+k+l,2(N+1)+m}\tag{28a}$$

and

$$\Delta_{jkl;m}^{(2)}=\delta_{-j+k+l,m}+\delta_{-j+k+l,-m}-\delta_{-j+k+l,2(N+1)-m}$$
$$+\delta_{j-k+l,m}+\delta_{j-k+l,-m}-\delta_{j-k+l,2(N+1)-m}$$
$$+\delta_{j+k-l,m}+\delta_{j+k-l,-m}-\delta_{j+k-l,2(N+1)-m}$$
$$+\delta_{j+k+l,m}-\delta_{j+k+l,2(N+1)-m}-\delta_{j+k+l,2(N+1)+m}.\tag{28b}$$

These Δ functions ensure the conservation of lattice momentum—the conservation of momentum to within the

nonuniqueness of the specification of the normal modes due to the fact that $\sin(nq_m)=\sin(nq_{2k(N+1)\pm m})$ for any integer k. The first Kronecker δ in each line is a condition of direct momentum conservation, and the other two are the so-called umklapp conditions, where only lattice momentum is conserved.

As for the single oscillator, we again try a steady-state solution, this time of the form

$$A_m(T)=a_m e^{i[(\Omega/2)-\Omega_m]T}, \tag{29}$$

so that the solutions to the EOM, after substitution of Eq. (29) into Eq. (21), become

$$x_n(t)=\epsilon^{1/2}\sum_m [a_m \sin(nq_m)e^{i(\omega_0+\epsilon\Omega/2)t}+\text{c.c.}]+O(\epsilon^{3/2}), \tag{30}$$

where all modes are oscillating at half the parametric excitation frequency $\omega_p/2$.

As before, we are not interested in the corrections of the order of $\epsilon^{3/2}$, but only in the values of the fixed amplitudes a_m as functions of all the parameters of the original EOM. Substituting the steady-state solution (29) into the Eq. (27) for the time-varying amplitudes $A_m(T)$, we obtain the required equations for the fixed complex amplitudes a_m

$$\begin{aligned}(\Omega-2\Omega_m)\omega_m a_m-2i\gamma\omega_m a_m\sin^2\left(\frac{q_m}{2}\right)+ha_m^*\sin^2\left(\frac{q_m}{2}\right)\\ -\frac{3}{4}\sum_{j,k,l} a_j a_k a_l^* \Delta^{(1)}_{jkl;m}-2i\eta\sin\frac{q_m}{2}\sum_{j,k,l}\omega_l[2a_j^* a_k a_l\\ -a_j a_k a_l^*]\sin\frac{q_j}{2}\sin\frac{q_k}{2}\sin\frac{q_l}{2}\Delta^{(2)}_{jkl;m}=0.\end{aligned} \tag{31}$$

We can change to rescaled variables as we did in the case of a single oscillator by dividing the equations for the amplitudes (31) by $(\gamma\omega_0)^{3/2}$ and defining as before $\overline{a_j}=a_j/\sqrt{\gamma\omega_0}$, $\overline{\Omega}=\Omega/\gamma$, $\overline{\eta}=\omega_0\eta$, and $\overline{h}=h/2\gamma\omega_0$, and in addition $r_m=\omega_m/\omega_0$ and $\delta_m=2\Omega_m/\gamma$. After doing so we obtain the rescaled equations

$$\begin{aligned}(\overline{\Omega}-\delta_m)r_m\overline{a}_m-2ir_m\sin^2\left(\frac{q_m}{2}\right)\overline{a}_m+2\overline{h}\sin^2\left(\frac{q_m}{2}\right)\overline{a}_m^*\\ -\frac{3}{4}\sum_{j,k,l}\overline{a}_j\overline{a}_k\overline{a}_l^*\Delta^{(1)}_{jkl;m}-2i\overline{\eta}\sin\frac{q_m}{2}\sum_{j,k,l} r_l[2\overline{a}_j^*\overline{a}_k\overline{a}_l\\ -\overline{a}_j\overline{a}_k\overline{a}_l^*]\sin\frac{q_j}{2}\sin\frac{q_k}{2}\sin\frac{q_l}{2}\Delta^{(2)}_{jkl;m}=0.\end{aligned} \tag{32}$$

This is the main result of the perturbative calculation. We have managed to replace N coupled differential equations (6) for the oscillator coordinates $x_n(t)$ by N coupled algebraic equations (31) for the time-independent mode amplitudes a_m. All that remains, in order to obtain the overall collective response of the array as a function of the parameters of the original EOM, is to solve these coupled algebraic equations.

Before doing so we should note the following general statements. First, one can easily verify that for a single oscillator ($N=j=k=l=m=1$), the general equation (31) reduces to the single-oscillator equation (15), we derived in Sec. III. Next, one can also see that the trivial solution, $a_m=0$ for all m, always satisfies the equations, though, as we have seen in the case of a single oscillator, it is not always a stable solution. Finally, one can also verify that whenever for a given m, $\Delta^{(1)}_{mmm;j}=\Delta^{(2)}_{mmm;j}=0$ for all $j\neq m$, then a single-mode solution exists with $a_m\neq 0$ and $a_j=0$ for all $j\neq m$. These single-mode solutions have the elliptical shape of the single-oscillator solution given in Eq. (17), and satisfy the equation

$$\begin{aligned}\frac{1}{4\sin^4(q_m/2)}\left(\frac{3}{4}\Delta^{(1)}_{mmm;m}|\overline{a}_m|^2-\overline{\Omega}\right)^2\\ +\left(1+\sin^2\frac{q_m}{2}\Delta^{(2)}_{mmm;m}\overline{\eta}|\overline{a}_m|^2\right)^2=\overline{h}^2,\end{aligned} \tag{33}$$

where for each solution we have set $\omega_0=\omega_m$, so that $\delta_m=0$ and $r_m=1$. Note that generically $\Delta^{(1)}_{mmm;m}=\Delta^{(2)}_{mmm;m}=3$, except when umklapp conditions are satisfied.

Additional solutions, involving more than a single mode, exist in general but are hard to obtain analytically. We calculate these multimode solutions below for the case of two and three oscillators by finding the roots of the coupled algebraic equations numerically. In Appendix B, we show the explicit sets of coupled mode-amplitude equations for these cases.

In Fig. 4, we show the solutions for the response intensity of two oscillators as a function of frequency, for a particular choice of the equation parameters. The top graph shows the square of the amplitude of the antisymmetric mode $\overline{a}_2$, whereas the bottom graph shows the square of the amplitude of the symmetric mode $\overline{a}_1$. Solid curves indicate stable solutions and dashed curves indicate unstable solutions. The two elliptical single-mode solution branches, mentioned in the previous paragraph are easily spotted. These branches are labeled by S_1 and S_2 [In Appendix B, Eqs. (B4), we give the analytical expressions for these two solution branches]. In addition, we find two double-mode solution branches, labeled D_1 and D_2, involving the excitation of both modes simultaneously. Note that the two branches of double-mode solutions intersect at a point where they switch their stability.

With two oscillators we obtain regions in frequency where three stable solutions can exist. If all the stable solution branches are accessible experimentally, then the observed effects of hysteresis might be more complex than in the simple case of a single oscillator. This is demonstrated in Fig. 5 where we compare our analytical solutions with a numerical integration of the differential equations of motion (6) for two oscillators. The response intensity, plotted here, is the time and space averages of the square of the oscillator displacements,

$$I=\frac{1}{N}\sum_{n=1}^{N}\langle x_n^2\rangle, \tag{34}$$

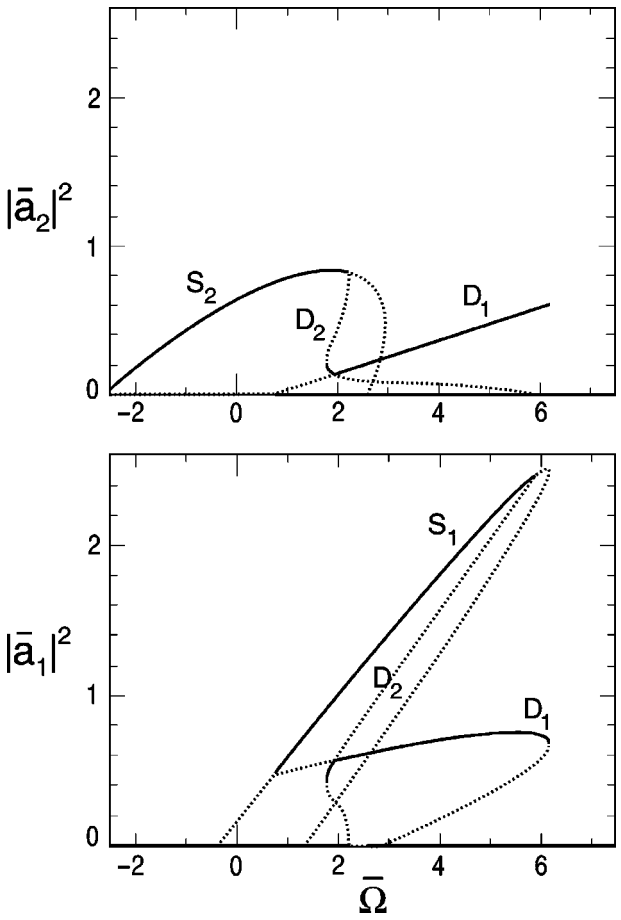

FIG. 4. Two oscillators: Response intensity of as a function of frequency $\bar{\Omega}$ for a particular choice of the equation parameters. The top graph shows $|\bar{a}_2|^2$ and the bottom graph shows $|\bar{a}_1|^2$. Solid curves indicate stable solutions and dashed curves indicate unstable solutions. The two elliptical single-mode solution branches [Eqs. (B4a) and (B4b)] are labeled S_1 and S_2. The two double-mode solution branches are labeled D_1 and D_2.

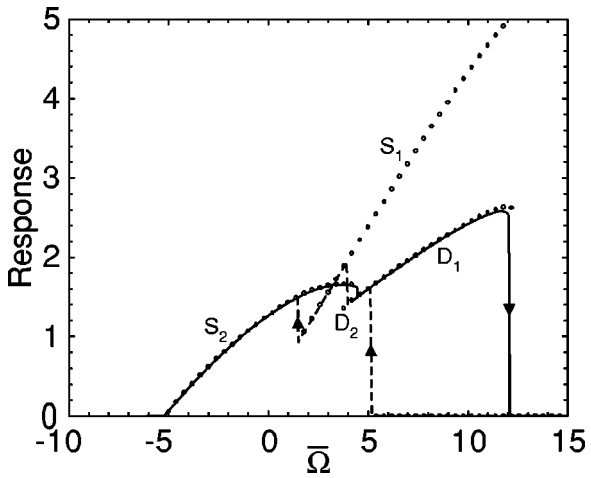

FIG. 5. Hysteresis with two oscillators: Comparison of stable solutions, obtained analytically (small circles), with a numerical integration of the equations of motion (solid curve - frequency swept up; dashed curve - frequency swept down). Plotted is the averaged response intensity, defined in Eq. (34). Branch labels correspond to those in Fig. 4.

where the angular brackets denote time average, and here $N=2$. A solid curve shows the response intensity for frequency swept upwards, and a dashed curve shows the response intensity for frequency swept downwards. Small circles show the analytical response intensity, using the fact that $I=3(|a_1|^2+|a_2|^2)/2$, for the stable regions of the four solution branches shown in Fig. 4. With the analytical solution in the background, one can easily understand all the discontinuous jumps, as well as the hysteresis effects, that are obtained in the numerical solution of the equations of motion. Note the the S_1 branch is missed in the upwards frequency sweep and is only accessed by the system in the downward frequency sweep. One could trace the whole stable region of the S_1 branch by changing the sweep direction after jumping onto the branch, thereby climbing all the way up to the end of the S_1 branch and then falling onto the tip of the D_1 branch or to zero.

In Fig. 6, we show the solutions for the response intensity of three oscillators as a function of frequency for a particular choice of the equation parameters. The graphs show the squares of the amplitudes of the three different modes. Solid curves indicate stable solutions and dashed curves indicate unstable ones. For three oscillators, there is only one elliptical single-mode solution branch, of the form of Eq. (33), whose exact analytical expression is given in Eq. (B8). This branch is labeled by S_2. In addition, we find a host of nontrivial multimode solution branches, including the one that is disconnected from all other branches. We show these plots, not only to demonstrate that it is possible to obtain such solutions exactly, but also to emphasize the large number and nontrivial structure of the solution branches one finds, even for such a small number of oscillators. This can only serve as a hint for the multimode solutions one can expect to find when the number of oscillators is large, as in the BR experiment.

V. RESPONSE OF PARAMETRICALLY DRIVEN NONLINEAR COUPLED OSCILLATORS—NUMERICAL INTEGRATION OF THE EQUATIONS

The equations of motion (6) were integrated numerically for an array of $N=67$ oscillators, as in the BR experiment. The results for the response intensity (34) as a function of parametric drive frequency ω_p (measured in units of the top band-edge frequency ω_0) are shown in Fig. 7. These results must be considered illustrative only, since many of the parameters of the experimental system are not known. The parameters used to construct the figure, $\Delta^2=0.02, \epsilon h=0.016$, $\epsilon\gamma=0.004$, and $\eta=6.0$, were chosen using the insights gained from the two- and three-oscillator results. We should emphasize that the structure of the response branches depends strongly on the equation parameters. First of all, as in the case of a small number of beams, the overall height and width of individual response branches depend on the strength of the drive h with respect to the linear damping coefficient γ, and on the nonlinear dissipation coefficient η. Further-

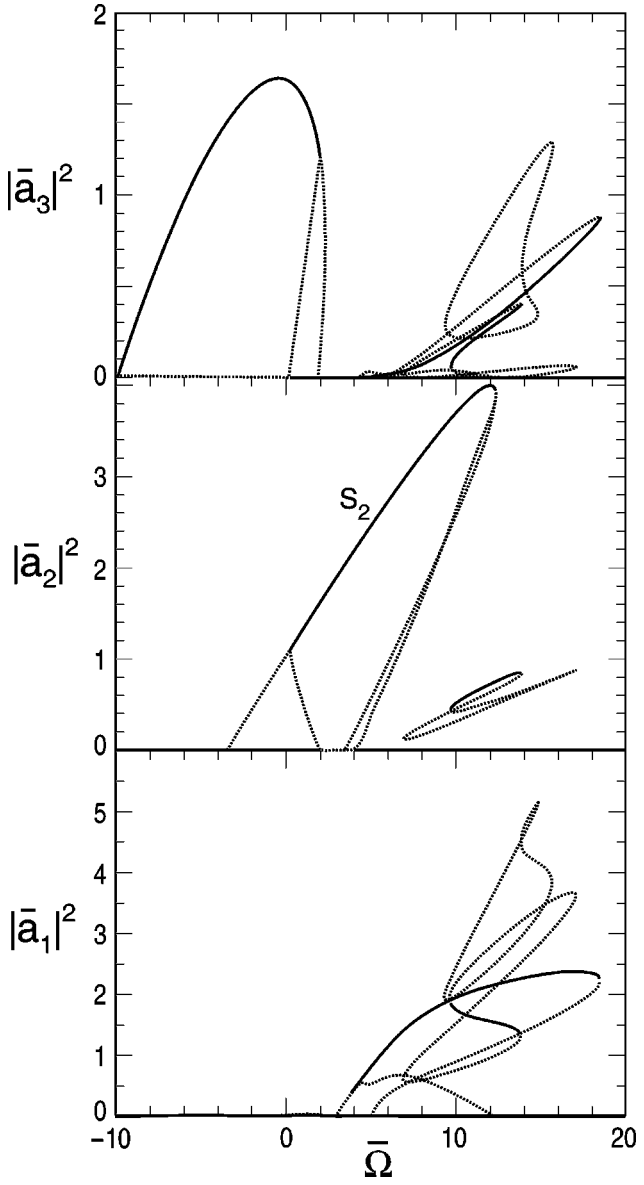

FIG. 6. Three oscillators: Response intensity of three oscillators as a function of frequency $\bar{\Omega}$ for a particular choice of the equation parameters. The graphs show the squares of the amplitudes of the three different modes. Solid curves indicate stable solutions and dashed curves indicate unstable ones. The only elliptical single-mode solution branch [Eq. (B8)] is labeled by S_2.

more, for example, if the width of the frequency response band is taken to be much larger than N times the width of a single-mode response, then very few multimode solutions exist, if any.

A number of the important features of the experimental data are reproduced by these calculations. We concentrate on the solid curve in the figure, which is for frequency swept upwards, since this is the protocol that was used in the experiment. In particular, the response intensity shows features that span a range of frequencies that is large compared with the mode spacing (which is about 0.0006 for the parameters used). The lowest-frequency feature, from about $\omega_p/\omega_0 = 1.94$ to $\omega_p/\omega_0 = 1.97$, can be identified as the response to

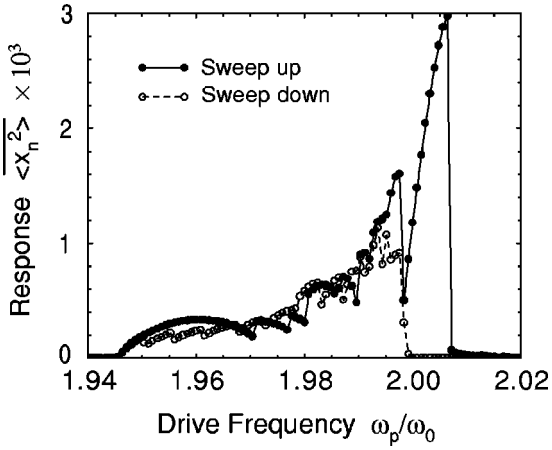

FIG. 7. Response intensity as a function of the driving frequency ω_p (measured in units of the top band-edge frequency ω_0) for $N=67$ parametrically driven oscillators (solid curve—frequency swept up; dashed curve—frequency swept down). The response intensity is defined as $\langle \overline{x_n^2} \rangle$ [Eq. (34)], with the bar denoting the average over the space index n, and the brackets the average over time. The parameters used are $\Delta^2=0.02$, $\epsilon h=0.016$, $\epsilon\gamma=0.004$, and $\eta=6$.

the parametric drive of a single mode at or very near the band edge at $\omega/\omega_0=0.98$, analogous to the one mode response shown in Fig. 1. Furthermore, the variation of the response with frequency shows abrupt jumps, particularly on the high-frequency side of the features as the frequency is raised. Finally, the response extends to frequencies higher than the band edge for the linear modes, which would give a response only up to $\omega_p/\omega_0=2.0$. All these features are understood, now that we have seen the analytical solutions for small numbers of oscillators. In particular, the wide features compared with the mode spacing are explained by the simple fact that as the frequency is swept upwards a particular solution branch is followed as long as it remains stable. In the meantime many other stable solutions that may be as close to each other as the mode spacing are simply skipped over.

Comparing the two traces in Fig. 7 shows that the response for a downward frequency sweep is significantly different with a less dramatic variation of the response. In particular, note that the downwards sweep was able to access additional stable solution branches that were missed in the upwards sweep. There is also no response above $\omega_p/\omega_0 = 2.0$ in this case. This is because the zero-displacement state is stable for $\omega_p/\omega_0 > 2.0$, and the system will remain in this state as the frequency is lowered, unless a large enough disturbance kicks it onto another of the solution branches. The hysteresis on reversing the frequency sweep was not looked at in the first experiments, and it would be interesting to test this prediction in further experiments.

VI. CONCLUSIONS

We have calculated the response of nonlinear coupled oscillators to parametric excitation. Our calculations agree qualitatively with the experimental measurements of Buks and Roukes[8] and explain the main features observed in the

experiment. The abrupt drops in the response as the frequency is swept upwards, the response continuing beyond the upper edge of the frequency band, and the large size of the response features compared with the mode spacing are all qualitatively explained.

Nevertheless, we propose that a more systematic study be conducted on systems of coupled nonlinear resonators so that our theoretical predictions could be tested more quantitatively. For example, successive measurements on systems containing only one, two, and three coupled resonators which are made as identically as possible, could be used to extract the nonlinear parameters of the resonators. These could then be used to predict and explain the response of a large resonator array more quantitatively.

Furthermore, we have demonstrated that as the number of oscillators is increased, the number of the solution branches for the response of the system increases and the effects of hysteresis become more and more complicated. This suggests that the appropriate experimental protocol for studying a system with many oscillators should be—in addition to the standard up-sweep and down-sweep in frequency—to change the direction of the sweep after every abrupt change in the response intensity. Such a protocol may provide more information about the response curve by accessing additional branches of the solution and fully tracing them out.

ACKNOWLEDGMENTS

This work was supported by Grant No. 1999458 from the U.S.-Israel Binational Science Foundation (BSF), and NSF Grant No. DMR-9873573. We thank Eyal Buks, Michael Roukes, and Inna Kozinsky for many useful discussions and for sharing their experimental results prior to publication.

APPENDIX A: PARAMETRIC EXCITATION OF A SINGLE OSCILLATOR AT ITS SECOND INSTABILITY TONGUE

For a single nonlinear oscillator, like the one studied in Sec. III, which is parametrically excited at its second instability tongue, Eq. (5) becomes

$$\ddot{x}+[\omega^2-\Delta^2 H\cos(\omega+\epsilon\Omega)t]x+\epsilon\gamma\dot{x}+x^3+\eta x^2\dot{x}=0, \tag{A1}$$

where again $\omega=\sqrt{1-\Delta^2}$ is the resonance frequency of the oscillator in the harmonic approximation, but the parametric excitation is performed around ω and not around 2ω. In this case, the scaling of $\Delta^2 H$ with respect to ϵ needs to be redetermined. The technical reason for this is that if we take $\Delta^2 H=\epsilon h$, as before, then the parametric driving term does not contribute to the order $\epsilon^{3/2}$ secular term that we use to find the response, and the order $\epsilon^{1/2}$ term in x becomes identically zero.

The remedy for this situation is to let $\Delta^2 H$ scale like ϵ^p with $p<1$, so that there will be a nonsecular correction to x at an order lower than $\epsilon^{3/2}$. The value of p will be chosen such that this correction will contribute to the order $\epsilon^{3/2}$ secular term and will give us the required response. The equation of motion (A1) becomes

$$\ddot{x}+\omega^2 x=\frac{h\epsilon^p}{2}(e^{i(\omega t+\Omega T)}+\text{c.c.})x-\epsilon\gamma\dot{x}-x^3-\eta x^2\dot{x}, \tag{A2}$$

and we try an expansion of the solution of the form

$$x(t)=\epsilon^{1/2}(A(T)e^{i\omega t}+\text{c.c.})+\epsilon^{p+1/2}x_p(t)+\epsilon^{3/2}x_1(t)+\cdots. \tag{A3}$$

Substituting this expansion into the equation of motion (A2), we obtain at the order $\epsilon^{1/2}$ the linear equation as usual, and at the order $\epsilon^{p+1/2}$

$$\ddot{x}_p+\omega^2 x_p=\frac{h}{2}(Ae^{i(2\omega t+\Omega T)}+A^*e^{i\Omega T}+\text{c.c.}). \tag{A4}$$

As expected, there is no secular term on the right-hand side, so we can immediately solve for x_p,

$$x_p(t)=\frac{h}{2}\left(-\frac{A}{3\omega^2}e^{i(2\omega t+\Omega T)}+\frac{A^*}{\omega^2}e^{i\Omega T}+\text{c.c.}\right)+O(\epsilon). \tag{A5}$$

Substituting the solution for x_p into the expansion (A3), and the expansion back into the equation of motion (A2), contributes an additional term from the parametric driving that has the form

$$\epsilon^{2p+1/2}\frac{h^2}{4}\left(-\frac{A}{3\omega^2}e^{i(2\omega t+\Omega T)}+\frac{A^*}{\omega^2}e^{i\Omega T}+\text{c.c.}\right)(e^{i(\omega t+\Omega T)}+\text{c.c.})=\epsilon^{2p+1/2}\frac{h^2}{4\omega^2}\left(\frac{2}{3}A+A^*e^{i2\Omega T}\right)e^{i\omega t}+\text{c.c.}+\text{nonsecular terms}. \tag{A6}$$

To contribute to the order $\epsilon^{3/2}$ secular term, we see that we must set $p=1/2$. This gives us the required contribution to the equation for the vanishing secular terms. All other terms remain as they were in Eq. (12), so that the new equation for determining $A(T)$ becomes

$$2i\omega\frac{dA}{dT}-\frac{h^2}{4\omega^2}\left(\frac{2}{3}A+A^*e^{i2\Omega T}\right)+i\omega\gamma A+3|A|^2A+i\omega\eta|A|^2A=0. \tag{A7}$$

Again, ignoring initial transients, and assuming that the nonlinear terms in the equation are sufficient to saturate the growth of the instability, we try a steady-state solution, this time of the form

$$A(T)=ae^{i\Omega T}. \tag{A8}$$

The solution to the equation of motion (A1) is therefore

$$x(t)=\epsilon^{1/2}(ae^{i(\omega+\epsilon\Omega)t}+\text{c.c.})+O(\epsilon), \tag{A9}$$

where the correction $x_{1/2}$ of order ϵ is given in Eq. (A5) and, as before, we are not interested in the correction $x_1(t)$ of the order of $\epsilon^{3/2}$, but rather in the fixed amplitude a of the lowest-order term. We substitute the steady-state solution (A8) into Eq. (A7) of the secular terms and obtain

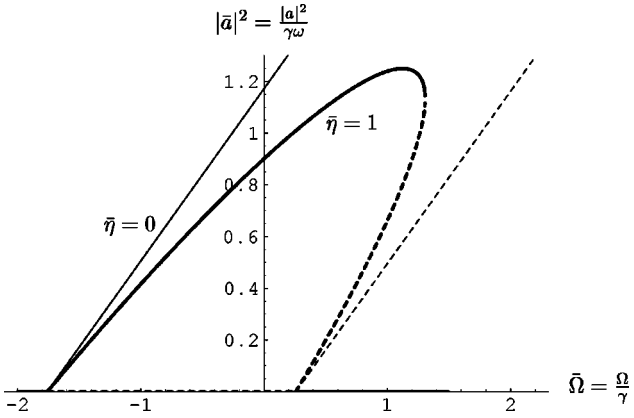

FIG. 8. Response intensity $|\bar{a}|^2$ as a function of the frequency $\bar{\Omega}$ for fixed amplitude $\bar{h}=1.5$ in the second instability tongue. Solid curves are stable solutions and dashed curves are unstable solutions. Thin curves show the response without non-linear damping ($\bar{\eta}=0$). Thick curves show the response for finite nonlinear damping ($\bar{\eta}=1$).

$$\left[\left(3|a|^2-2\omega\Omega-\frac{2}{3}\frac{h^2}{4\omega^2}\right)+i\omega(\gamma+\eta|a|^2)\right]a=\frac{h^2}{4\omega^2}a^*. \tag{A10}$$

We divide both sides of the last equation by $\gamma\omega$ and define the rescaled variables: $\bar{a}=a/\sqrt{\gamma\omega}$, $\bar{\Omega}=\Omega/\gamma$, $\bar{\eta}=\omega\eta$, and $\bar{h}=h/2\sqrt{\gamma\omega^3}$, in terms of which we obtain after taking the magnitude squared of both sides, in addition to the trivial solution $a=0$, the nontrivial response

$$\left(3|\bar{a}|^2-2\bar{\Omega}-\frac{2}{3}\bar{h}^2\right)^2+(1+\bar{\eta}|\bar{a}|^2)^2=\bar{h}^4. \tag{A11}$$

Figure 8 shows the response intensity $|\bar{a}|^2$ as a function of the frequency $\bar{\Omega}$ for fixed amplitude $\bar{h}=1.5$ in the second instability tongue. The solution looks very similar to the response shown in Fig. 1 for the first instability tongue, though we should point out two important differences. The first is that the orientation of the ellipse, indicated by the slope of the curves for $\bar{\eta}=0$, is different. The slope here is 2/3, whereas for the first instability tongue the slope is 1/3. The second is the change in the definition of $\bar{h}$. The lowest amplitude required for having an instability is again on resonance ($\bar{\Omega}=0$) and its value is again $\bar{h}=1$, but now this implies that $h=2\sqrt{\gamma\omega^3}$ or that h scales as $\sqrt{\gamma}$. This is consistent with the well-known result (see, for example, Ref. 10) that the minimal amplitude for the instability of the nth tongue scales as $\gamma^{1/n}$.

APPENDIX B: EXPLICIT EQUATIONS FOR TWO AND THREE COUPLED OSCILLATORS

1. Two coupled nonlinear oscillators

For two coupled oscillators ($N=2$), we have

$$q_1=\frac{\pi}{3},\quad q_2=\frac{2\pi}{3}, \tag{B1}$$

$$\omega_1^2=1-\frac{1}{2}\Delta^2,\quad \omega_2^2=1-\frac{3}{2}\Delta^2, \tag{B2}$$

and we choose the reference frequency ω_0 to be ω_2, so that $\delta_2=\Omega_2=0$, $r_2=1$, $\delta_1=2(\omega_1-\omega_2)/\gamma\epsilon\equiv\delta>0$, and $r_1=\omega_1/\omega_2\equiv r$. For $\Delta\ll 1$, $\delta\simeq\Delta^2/\epsilon\gamma$ and $r\simeq 1+\Delta^2/2$. The first mode is the symmetric one with $x_1(t)=x_2(t)$ and the second mode is antisymmetric with $x_1(t)=-x_2(t)$. Equations (32) for the rescaled complex amplitudes $\bar{a}_1$ and $\bar{a}_2$ are

$$(\bar{\Omega}-\delta)r\bar{a}_1-i\frac{r}{2}\bar{a}_1+\frac{\bar{h}}{2}\bar{a}_1^*-\frac{9}{4}(|\bar{a}_1|^2\bar{a}_1+2|\bar{a}_2|^2\bar{a}_1+\bar{a}_2^2\bar{a}_1^*)$$
$$-\frac{3}{8}i\bar{\eta}[r|\bar{a}_1|^2\bar{a}_1+2r|\bar{a}_2|^2\bar{a}_1+(2-r)\bar{a}_2^2\bar{a}_1^*]=0, \tag{B3a}$$

$$\bar{\Omega}\bar{a}_2-i\frac{3}{2}\bar{a}_2+\frac{3}{2}\bar{h}\bar{a}_2^*-\frac{9}{4}(|\bar{a}_2|^2\bar{a}_2+2|\bar{a}_1|^2\bar{a}_2+\bar{a}_1^2\bar{a}_2^*)$$
$$-\frac{3}{8}i\bar{\eta}[9|\bar{a}_2|^2\bar{a}_2+2|\bar{a}_1|^2\bar{a}_2+(2r-1)\bar{a}_1^2\bar{a}_2^*]=0. \tag{B3b}$$

The two single-mode solution branches, having the general form of Eq. (33) and labeled S_1 and S_2 in Fig. 4, are easily obtained by setting $\bar{a}_2$ or $\bar{a}_1$ to zero in the coupled equations above, respectively. This yields the analytical forms of these solutions, which are

$$S_1:\quad \left(\frac{9}{2}|\bar{a}_1|^2-2r(\bar{\Omega}-\delta)\right)^2+r^2\left(1+\frac{3}{4}\bar{\eta}|\bar{a}_1|^2\right)^2=\bar{h}^2, \tag{B4a}$$

$$S_2:\quad \left(\frac{3}{2}|\bar{a}_2|^2-\frac{2}{3}\bar{\Omega}\right)^2+\left(1+\frac{9}{4}\bar{\eta}|\bar{a}_2|^2\right)^2=\bar{h}^2. \tag{B4b}$$

2. Three coupled nonlinear oscillators

For three coupled oscillators ($N=3$) we have

$$q_1=\frac{\pi}{4},\quad q_2=\frac{\pi}{2},\quad q_3=\frac{3\pi}{4} \tag{B5}$$

$$\omega_1^2=1-\Delta^2+\frac{\Delta^2}{\sqrt{2}},\quad \omega_2^2=1-\Delta^2,\quad \omega_3^2=1-\Delta^2-\frac{\Delta^2}{\sqrt{2}}, \tag{B6}$$

and we choose the reference frequency ω_0 to be ω_2, so that $\delta_2=0$, $r_2=1$, and $\delta_1=2(\omega_1-\omega_2)/\gamma\epsilon=-\delta_3\equiv\delta>0$. For $\Delta\ll 1$, $\delta\simeq\Delta^2/\sqrt{2}\epsilon\gamma$ and $r_{1,3}\simeq 1\pm\Delta^2/2\sqrt{2}$. Equations (32) for the rescaled complex amplitudes $\bar{a}_1$, $\bar{a}_2$, and $\bar{a}_3$ are

$$(\bar{\Omega}-\delta)r_1\bar{a}_1-i\frac{2-\sqrt{2}}{2}r_1\bar{a}_1+\frac{2-\sqrt{2}}{2}\overline{ha_1^*}-\frac{3}{4}(3|\bar{a}_1|^2\bar{a}_1-|\bar{a}_3|^2\bar{a}_3+4|\bar{a}_2|^2\bar{a}_3+2\bar{a}_2^2\bar{a}_3^*+4|\bar{a}_2|^2\bar{a}_1+2\bar{a}_2^2\bar{a}_1^*+6|\bar{a}_3|^2\bar{a}_1$$
$$+3\bar{a}_3^2\bar{a}_1^*-2|\bar{a}_1|^2\bar{a}_3-\bar{a}_1^2\bar{a}_3^*)-i\eta\left[\frac{3-2\sqrt{2}}{4}3r_1|\bar{a}_1|^2\bar{a}_1-\frac{\sqrt{2}+1}{4}r_3|\bar{a}_3|^2\bar{a}_3+\frac{2-\sqrt{2}}{2}[2r_1|\bar{a}_2|^2\bar{a}_1+(2-r_1)\bar{a}_2^2\bar{a}_1^*]\right.$$
$$\left.+\frac{\sqrt{2}-1}{4}[2r_3|\bar{a}_1|^2\bar{a}_3+(2r_1-r_3)\bar{a}_1^2\bar{a}_3^*]+\frac{1}{4}[2r_1|\bar{a}_3|^2\bar{a}_1+(2r_3-r_1)\bar{a}_3^2\bar{a}_1^*]\right]=0, \tag{B7a}$$

$$\bar{\Omega}\bar{a}_2-i\bar{a}_2+\overline{ha_2^*}-\frac{3}{2}(2|\bar{a}_2|^2\bar{a}_2+2|\bar{a}_1|^2\bar{a}_2+\bar{a}_1^2\bar{a}_2^*+2|\bar{a}_3|^2\bar{a}_2+\bar{a}_3^2\bar{a}_2^*+\bar{a}_1^*\bar{a}_2\bar{a}_3+\bar{a}_1\bar{a}_2^*\bar{a}_3+\bar{a}_1\bar{a}_2\bar{a}_3^*)$$
$$-i\eta\left[|\bar{a}_2|^2\bar{a}_2+\frac{2-\sqrt{2}}{2}[2|\bar{a}_1|^2\bar{a}_2+(2r_1-1)\bar{a}_1^2\bar{a}_2^*]+\frac{2+\sqrt{2}}{2}[2|\bar{a}_3|^2\bar{a}_2+(2r_3-1)\bar{a}_3^2\bar{a}_2^*]\right]=0, \tag{B7b}$$

$$(\bar{\Omega}+\delta)r_3\bar{a}_3-i\frac{2+\sqrt{2}}{2}r_3\bar{a}_3+\frac{2+\sqrt{2}}{2}\overline{ha_3^*}-\frac{3}{4}(3|\bar{a}_3|^2\bar{a}_3-|\bar{a}_1|^2\bar{a}_1+4|\bar{a}_2|^2\bar{a}_3+2\bar{a}_2^2\bar{a}_3^*+4|\bar{a}_2|^2\bar{a}_1+2\bar{a}_2^2\bar{a}_1^*+6|\bar{a}_1|^2\bar{a}_3$$
$$+3\bar{a}_1^2\bar{a}_3^*-2|\bar{a}_3|^2\bar{a}_1-\bar{a}_3^2\bar{a}_1^*)-i\eta\left[\frac{3+2\sqrt{2}}{4}3r_3|\bar{a}_3|^2\bar{a}_3+\frac{\sqrt{2}-1}{4}r_1|\bar{a}_1|^2\bar{a}_1+\frac{2+\sqrt{2}}{2}[2r_3|\bar{a}_2|^2\bar{a}_3+(2-r_3)\bar{a}_2^2\bar{a}_3^*]\right.$$
$$\left.-\frac{\sqrt{2}+1}{4}[2r_1|\bar{a}_3|^2\bar{a}_1+(2r_3-r_1)\bar{a}_3^2\bar{a}_1^*]+\frac{1}{4}[2r_3|\bar{a}_1|^2\bar{a}_3+(2r_1-r_3)\bar{a}_1^2\bar{a}_3^*]\right]=0. \tag{B7c}$$

Only one single-mode solution of the form of Eq. (33) exists in the case of three oscillators and involves the second mode. It is obtained by setting $\bar{a}_1=\bar{a}_3=0$ in the coupled equations above. The analytical expression for this solution is

$$S_2: \quad (3|\bar{a}_2|^2-\bar{\Omega})^2+(1+\overline{\eta}|\bar{a}_2|^2)^2=\overline{h^2}. \tag{B8}$$

[1] M.L. Roukes, Phys. World **14**(2), 25 (2001).
[2] H.G. Craighead, Science **290**, 1532 (2000).
[3] M.L. Roukes, Sci. Am. **285**(3), 42 (2001).
[4] E. Buks and M.L. Roukes, Europhys. Lett. **54**, 220 (2001).
[5] D. Rugar and P. Grütter, Phys. Rev. Lett. **67**, 699 (1991).
[6] D.A. Harrington and M.L. Roukes (unpublished).
[7] D.W. Carr, S. Evoy, L. Sekaric, H.G. Craighead, and J.M. Parpia, Appl. Phys. Lett. **77**, 1545 (2000).
[8] E. Buks and M.L. Roukes, J. Microelectromech. Syst. **11**, 802 (2002).
[9] E. Buks (private communication).
[10] L.D. Landau and E.M. Lifshitz, *Mechanics*, 3rd ed. (Butterworth-Heinemann, Oxford, 1976), Sec. 27.
[11] G. Litak, G. Spuz-Szpos, K. Szabelski, and J. Warminski, Int. J. Bifurcation Chaos **9**, 493 (1999).
[12] S.H. Strogatz, *Nonlinear Dynamics and Chaos* (Addison-Wesley, Reading, MA, 1994), Chap. 7.
[13] L.N. Hand and J.D. Finch, *Analytical Mechanics* (Cambridge University Press, Cambridge, 1998), Chap. 10.